Polymer Journal, Vol. 24, No. 9, pp 899—916 (1992)

Vibrational Spectra and Theoretical Three-Dimensional Elastic Constants of Isotactic Polypropylene Crystal: An Important Role of Anharmonic Vibrations

Kohji TASHIRO,* Masamichi KOBAYASHI, and Hiroyuki TADOKORO

Department of Macromolecular Science, Faculty of Science, Osaka University, Toyonaka, Osaka 560, Japan

(Received January 10, 1992)

ABSTRACT: Calculation of normal mode frequencies and three-dimensional elastic constants is made for the first time for isotactic polypropylene crystal on the basis of lattice dynamical theory. The vibrational frequencies are found in relatively good agreement with the observed values for both the internal and external modes. The calculated Young's modulus along the chain axis is 40.1 GPa which agrees well with the X-ray observed crystallite modulus *ca.* 40 GPa. The anisotropic curves of Young's modulus and linear compressibility in the plane perpendicular to the chain axis are also calculated but agreement with the values observed at room temperature is not good. This discrepancy is erased successfully by considering a large anharmonic effect of methyl torsional modes.

KEY WORDS Isotactic Polypropylene Crystal / Infrared Spectra / Raman Spectra / Normal-Coordinates Treatment / Three-Dimensional Elastic Constants / Lattice Dynamics / Anharmonicity /

In recent years many trials have been made to produce fully extended fibers with ultra high modulus and strength.[1,2] Such a trial may be classified into two types. One is to utilize the so-called rigid-rod polymers. For example, poly(*p*-phenylene benzobisthiazole) (PBT) and poly(*p*-phenylene benzobisoxazole) (PBO) show the bulk tensile moduli of about 330 and 420 GPa, respectively.[3] Further development of fibers with higher modulus is still being tried so as to approach the limiting Young's modulus or crystallite modulus: 395 GPa (observed[4]) and 405 GPa (calculated[5]) for PBT and 477 GPa (observed[4]) and 460 GPa (calculated[5]) for PBO. Another trial to produce ultra high modulus fibers is usage of flexible polymers. Young's modulus of polyethylene fiber, for example, was reported to reach about 230 GPa at room temperature by drawing the dried gels by several hundred times the original length[6]. This value is close to the limiting modulus of the crystalline region, 250—310 GPa.[7,8] Such a trial has been also made for isotactic polypropylene (it-PP) and the Young's modulus of about 40 GPa was reported for the ultra-drawn fibers.[9,10] This macroscopic modulus is comparable to the crystallite modulus *ca.* 40 GPa.[7,11] In these studies we may notice that evaluation of the limiting modulus is very important as a guiding principle to develop more mechanically qualified samples.

Experimentally, the limiting modulus of polymer crystal is estimated mainly by the X-ray diffraction measurement under tension.[7] An alternative method is evaluation of velocity of phonon propagating in the polymer crystal, which can be made by measuring the Raman LAM band[12] (LAM: longitudinal acoustic mode) or the frequency-dispersion curve by neutron scattering experiment.[13] Thus evaluated limiting modulus must be interpreted from the molecular theoretical point of view in terms of crystal structure and intramolecular and intermolecular interactions. Such a theo-

retical approach is very difficult for polymer crystals with complicated structure. In a series of papers,[14] we developed lattice dynamical equations to calculate the three-dimensional elastic constants of polymer crystals such as orthorhombic polyethylene,[8,15] poly(vinyl alcohol),[8] nylon 6α and γ forms,[16] poly(vinylidene fluoride),[17] cellulose I and II forms,[18] and poly(*m*-phenylene isophthalamide),[18] the mechanical anisotropy of which was discussed based on molecular and crystal structures. In these calculations, symmetry relations between crystallographically asymmetric units in the unit cell are utilized and therefore the dimensions of matrices used in the numeric calculation can be reduced drastically.[15] This reduction makes it possible to calculate the three-dimensional elastic constants of polymer crystals with complicated structures and increases reliabilility of the calculated results because of simpler and more confirmative preparation of input data necessary for computer calculation. The calculation is based on the three-dimensional Cartesian coordinate system, which makes it possible to reserve the translational symmertry of the crystal lattice even under application of external stress.[15,19,20]

In this paper we focus attention on it-PP crystal and estimate the three-dimensional elastic constants on the basis of thus developed lattice dynamical theory. In spite of its significance in industrial and scientific fields, no trial has been reported so far for it-PP crystal on the calculation of three-dimensional elastic constants as well as on the calculation of the normal modes frequencies of both the internal and external vibrational modes. One of the reasons may come from the complicated crystal structure. Calculation of normal modes frequencies is necessary for correct estimation of the intramolecular and intermolecular force fields of the it-PP crystal, which will definitely guarantee the calculated results of three-dimensional elastic constants.

Before details of the calculated results are described, it is considered to be useful to briefly review the structural and spectroscopic studies reported so far for it-PP crystal, because these informations may help us to carry out the calculation with a use of reasonable structural and interaction parameters.

Crystal Structure of it-PP

Natta and Corradini[21] analysed the X-ray fiber photograph of it-PP and proposed the two kinds of crystal structural models with space groups $C2/c$ and Cc. In the unit cell of $C2/c$, the molecular chains of (3/1) helical conformation are packed upward and downward with an equal statistical weight. In the unit cell of Cc, the chain packing is regular. They could not, however, determine which structural model is more reasonable, but speculated that the molecular chains in local domains are packed in a regular mode of the space group symmetry Cc and these domains are aggregated at random in the crystallites, resulting in an overall space group symmetry of $C2/c$. Mencik[22] found several X-ray reflections unexplainable by the space group $C2/c$ and proposed a structure of the space group $P2_1/c$ for an ideally ordered state. At the same time he investigated a crystal structural model in the actual sample, which is an averaged structure consisting of the ordered ($P2_1/c$) and disordered ($C2/c$) chain packing with statistical weight of *ca.* 3:1. Independently, Hikosaka and Seto[23] indexed the observed X-ray reflections based on the space group $C2/c$ for the sample annealed at relatively low temperature and on the space group $P2_1/c$ for the sample annealed at higher temperature. That is, the packing regularity changes remarkably by heat treatment of the sample; the intensity of the X-ray spots characteristic of the space group $P2_1/c$ increases gradually with a rise of annealing temperature and the regular structural domains grow in size within irregular crystallites of the space group symmetry $C2/c$. In other words, the it-PP crystal experiences a kind of

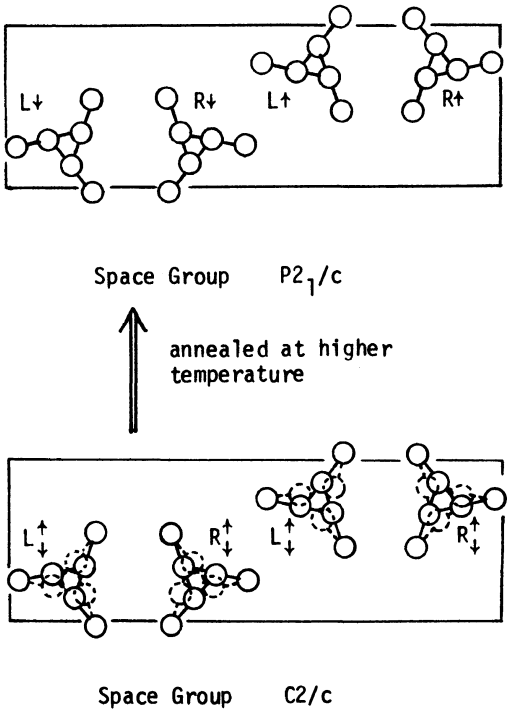

Figure 1. Structures of ordered ($P2_1/c$) and disodered ($C2/c$) crystal states of it-PP.

disorder-order phase transition induced by the heat treatment as illustrated in Figure 1.

Vibrational Analysis of it-PP

Information on intramolecular and intermolecular interactions, necessary for the present calculation, can be obtained from the normal modes analysis of infrared and Raman spectra. Vibrational analyses of it-PP have been reported by many investigators mainly for an isolated chain. Normal coordinates treatments were made for a (3/1) helical chain by Snyder and Schachtschneider,[24] Miyazawa,[25] Tadokoro *et al.*,[26] and Zerbi and Piseri.[27] In the low frequency region of skeletal torsional modes and external lattice modes, Raman spectral measurements were reported by Fraser *et al.*[28] and far-infrared spectral data by Goldstein *et al.*[29] But the normal mode calculation including the lattice vibrational modes with both the intramolecular and intermolecular interactions taken into account has not been reported so far. This may be because of the complexity of the crystal structure of it-PP. In this paper we report the first normal modes treatment of it-PP crystal and compare the calculated results with the observed spectral data in the frequency region of 4000—30 cm^{-1}. Based on thus checked intramolecular and intermolecular force constants, the three-dimensional elastic constants are calculated and compared with the observed data.

EXPERIMENTAL

it-PP samples used in the spectral measurements were supplied from Mitsui Petrochemical Industry Co., Ltd. and Sumitomo Chemicals Co., Ltd. in Japan. For measurements of polarized far-infrared spectra, oriented films of 1.5 mm thickness were prepared by elongating the melt-quenched plates by five times the original length at *ca.* 100°C. For the unpolarized far-infrared spectra the unoriented plates of thickness *ca.* 5 mm were utilized. These samples were annealed at a temperature of 100—165°C. For the samples used in the Raman spectral measurements, rod specimens, prepared by extrusion of the melt through the glass cylinder, were elongated by about 5 times the original length at about 110°C and annealed at various temperatures under tension.

Far-infrared spectra were measured by a Hitachi FIS-3 far-infrared spectrophotometer for the frequency region 400—30 cm^{-1}. Polarized Raman spectra were measured at room temperature and liquid nitrogen temperature using a Japan Spectroscopic Company R500 Raman spectrophotometer with an argon ion laser of 514.5 nm wavelength as an excitation light source.

CALCULATIONS OF NORMAL MODE FREQUENCIES AND ELASTIC CONSTANTS

Calculation of lattice vibrational frequencies

and elastic constant tensors was made on the basis of the three-dimensional Cartesian coordinates system. The dynamical equation for the normal mode frequencies is given as[30]

$$|\boldsymbol{M}^{-1/2}\tilde{\boldsymbol{B}}\boldsymbol{F}_{\mathrm{R}}\boldsymbol{B}\boldsymbol{M}^{-1/2}-\lambda\boldsymbol{E}|=0 \qquad (1)$$

where $\boldsymbol{F}_{\mathrm{R}}$, $\boldsymbol{B}$, and $\boldsymbol{M}$ are matrices related to the force constants, geometry, and atomic masses, respectively. $\boldsymbol{E}$ is an identity matrix and λ is an eigenvalue. The elastic constant tensor $\boldsymbol{c}$ is obtained by the following equation.[15]

$$\boldsymbol{c}=(1/v)[\boldsymbol{F}_{\sigma}-\tilde{\boldsymbol{F}}_{\rho\sigma}(\boldsymbol{F}_{\rho})^{-1}\boldsymbol{F}_{\rho\sigma}] \qquad (2)$$

where v is the volume of asymmetric unit and $\boldsymbol{F}_{\sigma}$, $\boldsymbol{F}_{\rho\sigma}$, and $\boldsymbol{F}_{\rho}$ are the matrices constructed by the atomic coordinates, $\boldsymbol{B}$-matrix, and force constants. As can be seen in eqs 1 and 2, the vibrational frequencies and elastic constants can be calculated simultaneously using a set of structual parameters and force constants. In other words, we may obtain the calculated elastic constants as reasonably as possible by using the $\boldsymbol{B}$ and $\boldsymbol{F}_{\mathrm{R}}$ matrices checked by a comparison of observed and calculated vibrational frequencies. Utilized structural and force field parameters are described below. It should be noted here that the structural unit required for these calculations is only one crystallographic asymmetric unit and all parameters for whole unit cell are not necessary because of space group symmetry.

Crystal Structure

The crystal structure model proposed by Hikosaka and Seto[23] (space group $P2_1/c$) was used for the highly ordered crystal state (Figure 1). The unit cell parameters are $a=6.65$ Å, $b=20.73$ Å, c (fiber axis)$=6.50$ Å and $\beta=98°40'$. For a low-order state, the molecular chains directing upwards and downwards along the chain axis were positioned at each site of the cell with a statistical weight 0.5, where unit cell parameters were assumed the same with those of the regular state. Hydrogen atoms of the CH_2 and CH groups were assumed located at the positions determined by

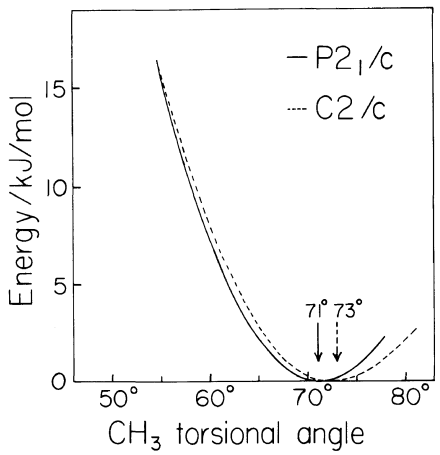

Figure 2. Calculated potential energy as a function of torsional angle of methyl groups. ——, ordered state ($P2_1/c$); ------, disordered state ($C2/c$).

the conditions of ∠HCH (∠HCMe)$=109.5°$, ∠HCC$=$∠HCC $(+1)$ and C–H$=1.09$ Å. The positions of hydrogen atoms of methyl (Me) groups were determined so that the lattice energy became minimal. In this energy calculation, the skeletal chain conformation was given from the X-ray crystallographic data and kept unchanged. The rotational angles of three Me groups contained in the repeating period of the chain were assumed to be equal although the actual molecular chains are not required to have any 3_1 helical symmetry in the unit cell. The interactions considered in the lattice sum calculation were Me torsional barrier,

$$V_{\tau}=V_{\mathrm{o}}(1+\cos 3\tau)/2 \qquad (3)$$

where τ is a torsional angle and $V_{\mathrm{o}}=8.36$ kJ mol^{-1}, and the non-bonded interatomic interactions of Buckigham type potential

$$V_{\mathrm{r}}=A/r^6+B\exp(-Cr) \qquad (4)$$

for all atomic pairs of H$\cdots$H, H$\cdots$C and C$\cdots$C with the interatomic distance shorter than 20 Å. Numerical values of the parameters A, B, and C were taken from Williams' set IV (For H$\cdots$H, $A=-114.1$ kJ Å^6 mol^{-1}, $B=11094$ kJ mol^{-1}, $C=3.74$ Å^{-1}; for H$\cdots$C, $A=$

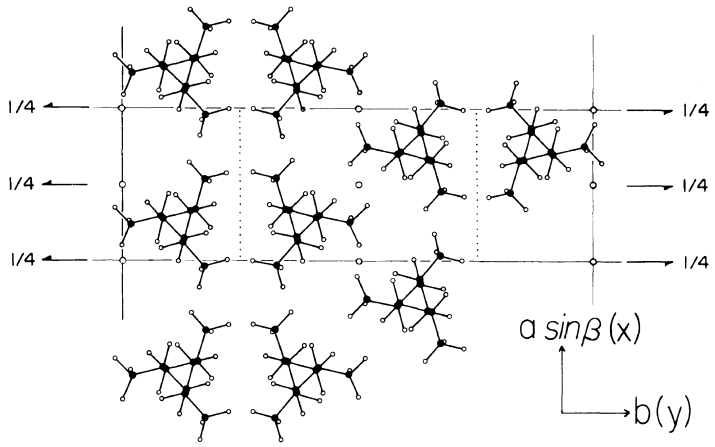

Figure 3. Crystal structure of ordered state of it-PP, where torsional angles of methyl groups are minimized as shown in Figure 2.

-522.5, $B=36642$, $C=3.67$; and for C$\cdots$C, $A=-2374.2$, $B=349573$, $C=3.60$).[31,32] Figure 2 shows the calculated potential energy as a function of the internal rotation angle τ(Me). An energy minimum is found at $\tau=71°$ for the $P2_1/c$ structure. For the disordered structure, the angle 73° gives the energy minimum. Figure 3 illustrates the energetically minimal crystal structure of the ordered phase.

Force Field

For intramolecular force constants a modified Urey-Bradley type was used, numerical values of which were quoted from references 25 and 26 with some modifications as shown in Table I. For the intermolecular force constants the second derivatives of Buckingham type potentials [eq 4] with respect to the distance r were used for all the intermolecular interatomic pairs with distance shorter than 4 Å.

RESULTS AND DISCUSSION

A. Vibrational Analyses of it-PP Crystal

Most papers reported so far treated only the normal modes of the it-PP single chain, where the molecular conformation was assumed to have the 3_1 screw symmetry along the chain axis. The factor group of the chain is isomorphous to point group C_3. But, as stated in the introductory section and Figure 3, the actual crystal belongs to the space group $P2_1/c$ and so the molecular chain has no such symmetry element as 3_1 helix but the site group symmetry is C_1. A correlation between these symmetry groups is obtained as follows.

Molecular group symmetry C_3	Site group symmetry C_1	Space group symmetry C_{2h}
$A\,[\alpha'_{xx},\alpha'_{yy},\alpha'_{zz},\alpha'_{xy};\mu'_z]$	A	$A_g\,[\alpha'_{aa},\alpha'_{bb},\alpha'_{cc},\alpha'_{ac}]$
		$B_g\,[\alpha'_{ab},\alpha'_{bc}]$
$E[(\alpha'_{yz},\alpha'_{xz});(\mu'_x,\mu'_y)]$		$A_u[\mu'_b]$
		$B_u[\mu'_a,\mu'_c]$

Here the z and c axes are parallel to the chain axis. α'_{xx}, α'_{aa}, etc. represent the Raman-active polarization components and μ'_x, μ'_a, etc. represent the infrared-active transition dipole components. As can be seen in this correlation table, the degenerated E modes split into two bands due to lowering of the molecular symmetry at the lattice site (site group splitting). Furthermore all molecular modes should split into four bands because of the phase relation among the four chains in the

Table I. Urey–Bradley-type intramolecular force constants of it-PP

Force constants[a]	Related atoms[b] (examples)	Values[c]
K(CH, Me)	(5, 7)	4.255
K(CH, CH_2)	(1, 2)	3.980
K(CH, CH)	(4, 6)	4.030
K(CC)	(1, 4), (4, 5)	2.470
H(CCC)	(1, 4, 10)	0.350
H(CCH, Me)	(4, 5, 7)	0.221
H(CCH)	(3, 1, 4)	0.240
H(CCH)	(1, 4, 6)	0.249
H(HCH, Me)	(7, 5, 8)	0.407
H(HCH, CH_2)	(2, 1, 3)	0.387
H(CCH, CH)	(6, 4, 5)	0.309
F(H···H, Me)	(7, 8)	0.100
F(H···H, CH_2)	(2,3)	0.121
F(C···H, Me)	(7, 4)	0.433
F(C···H, CH_2)	(2, 4)	0.433
F(C···H, CH)	(6, 5), (6.1)	0.400
F(C···C)	(1, 10), (1, 5)	0.200
κ(Me)	Intramolecular tension	−0.030
κ(CH_2)	Intramolecular tension	−0.020
κ(CH)	Intramolecular tension	0.030
T(CCCC)	(0, 1, 4, 10)	0.176

[a] K, bond stretching; H, bond angle deformation; F, interatomic repulsion (geminal atomic pairs); κ, intramolecular tension; T, skeletal torsion. Refer to ref 25 and 26.

[b] Numbering of atoms is an follows:

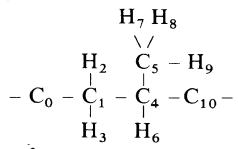

[c] Units, mdyn Å^{-1} for K, H, F, κ, and T, mdyn Å rad^{-2}.

unit cell (Davidov splittings): two bands (A_g and B_g) are active in the Raman spectra and the other two (A_u and B_u) are active in the infrared spectra. As for the lattice vibrational modes, 13 bands in total are expected to be observed in the Raman or infrared spectra. In Figure 4 are illustrated the lattice vibrational modes. Figures 5 and 6 show examples of the observed far-infrared and Raman spectra, respectively. The calculated vibrational frequencies of it-PP crystal are listed in Table II. A partial comparison of the calculated frequencies with the observed data is made in Figure 4 (lattice vibrations) and in Figure 5

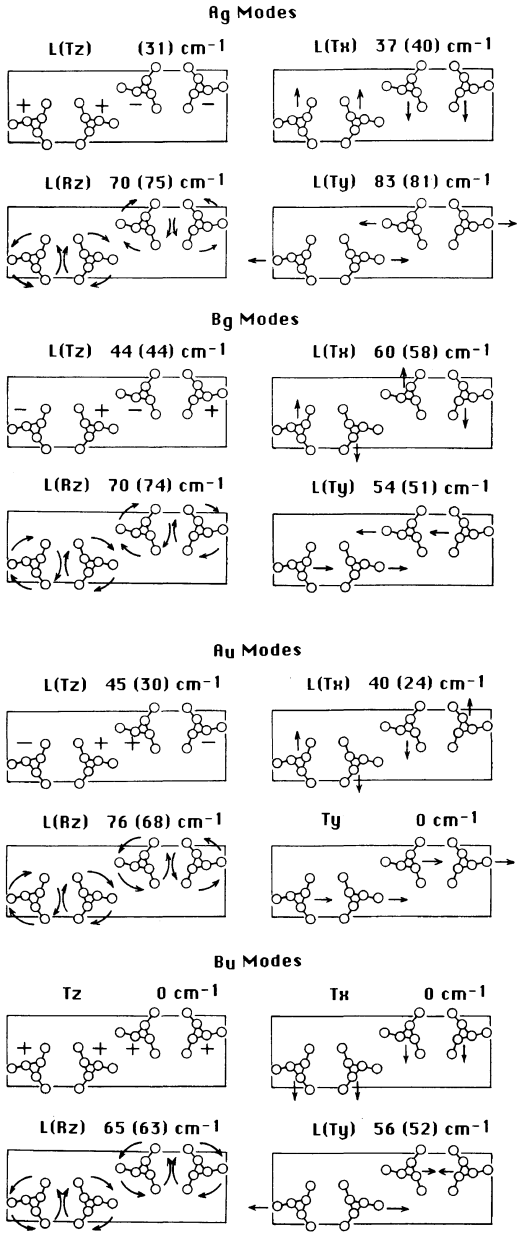

Figure 4. Lattice vibrational modes of it-PP crystal ($P2_1/c$). Indicated wavenumbers are the observed values and those in parentheses are the calculated ones.

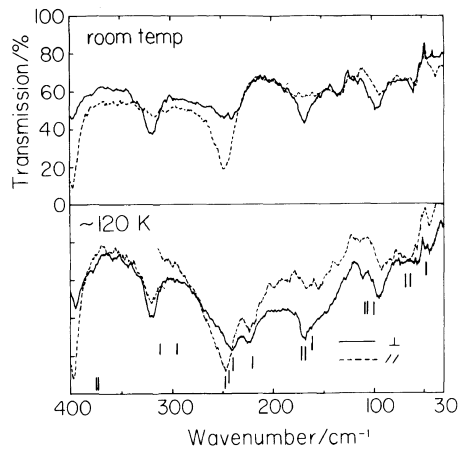

Figure 5. Polarized far-infrared spectra of it-PP measured at room temperature and at liquid nitrogen tempeature. ——, electric vector of incident infrared beam is perpendicular to the draw direction; ------, electric vector of incident infrared beam is parallel to the draw direction. Vertical rods indicate the positions of the calculated vibrational modes (refer to in Table II).

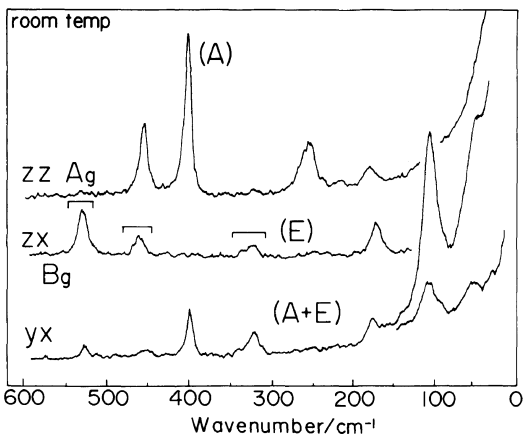

Figure 6. Polarized Raman spectra of it-PP measured at room temperature. The z axis is parallel to the draw direction of the sample and the x and y axes are perpendicular to it.

(far-infrared spectra at low temperature). Refer to ref 24—27 for comparison in the higher frequency region because the calculated frequencies are not so different from them. As pointed out above, the originally degenerated E modes split into two bands due to symmetry lowering of the helical chain conformation. In Table II, we can see some pairs of modes which seem to originate from E modes of C_3 group. They are indicated in parentheses in this table. The calculated site-group splittings are in the range of 0 to 8 cm^{-1}. In polarized Raman spectra of the component (xz) in Figure 6, some pairs, *e.g.*, 320 and 325 cm^{-1}, 462 and 470 cm^{-1}, etc. are considered to come from such a site group splitting because these bands are detected as doublets even at room temperature. On the other hand, by comparing the frequencies of four symmetry species (A_g, B_g, etc.) in Table II, we can predict that intramolecular vibrational modes should split by a magnitude of 0—5 cm^{-1} due to the intermolecular interactions. As reported by Fraser *et al.*,[28] however, Davidov splitting is actually difficult to be observed even at 5 K. Methyl torsional bands τ (Me) should also not be overlooked here. As shown in Table II, the calculated frequencies of τ(Me) disperse in a relatively wide range of 220 to 260 cm^{-1} in a complicated manner. Originally the calculated results should be compared with the spectra measured at low temperature. This is because the methyl groups are said to experience rather violent rotational motion at room temperature[33] and such a motion is considered to reduce the anisotropy in intermolecular interactions and thus the band profile should be rather simple at room temperature. At low temperature, however, the methyl motions are suppressed and the spectra should be more complicated and composed of several split bands as predicted by the lattice modes calculation where thermally excited large-amplitude motion is not taken into consideration. In fact, as shown in far-infrared spectra of Figure 5, bands in the 200—300 cm^{-1} region changes drastically as the temperature is decreased. An apparently singlet band at room temperature split into a complicated profile.[34] In particular, such a change is enhanced more remarkably below -145°C as shown in Figure 7, where the temperature dependence of the spectra in 200—300 cm^{-1} region is reproduced.

Table II. Vibrational frequencies calculated for it-PP crystal[a]

Modes[b]	Species	ν_{calc}/cm^{-1}					
$\nu_a(CH_3)$	A_g	2913	2911	2908	2907	2905	2904
	B_g	2913	2910	2910	2908	2907	2905
	A_u	2913	2910	2910	2908	2907	2905
	B_u	2913	2911	2908	2907	2905	2904
ν(CH)	A_g	2895	2892	2889			
	B_g	2895	2891	2889			
	A_u	2895	2891	2889			
	B_u	2895	2892	2889			
$\nu_s(CH_3)$	A_g	2866	2865	2863			
	B_g	2865	2864	2862			
	A_u	2865	2864	2862			
	B_u	2865	2865	2863			
$\nu_a(CH_2)$	A_g	2862	2859	2857			
	B_g	2861	2860	2857			
	A_u	2860	2858	2857			
	B_u	2859	2858	2857			
$\nu_s(CH_2)$	A_g	2841	2839	2837			
	B_g	2841	2839	2836			
	A_u	2840	2838	2835			
	B_u	2840	2838	2835			
$\delta_a(CH_3)$	A_g	1476					
$+\delta$(CH)	B_g	1476					
	A_u	1474					
	B_u	1474					
$\delta_a(CH_3)$	A_g	(1461	1460)	1459	(1459	1458)	1456
	B_g	(1462	1461)	1459	(1459	1459)	1455
	A_u	(1462	1460)	1459	(1459	1455)	1455
	B_u	(1460	1460)	1459	(1458	1456)	1455
$\delta(CH_2)$	A_g	1429	(1421	1419)			
$+\delta$(CH)	B_g	1429	(1420	1419)			
	A_u	1429	(1421	1419)			
	B_u	1429	(1421	1419)			
δ(CH)	A_g	(1418	1413)				
$+\delta(CH_2)$	B_g	(1417	1413)				
	A_u	(1417	1413)				
	B_u	(1418	1413)				
δ(CH)+	A_g	1383					
$\delta_s(CH_3)$	B_g	1383					
	A_u	1383					
	B_u	1383					
$\delta_s(CH_3)$	A_g	(1360	1358)				
	B_g	(1360	1359)				
	A_u	(1360	1358)				
	B_u	(1359	1358)				
$\omega(CH_2)$	A_g	1356	(1351	1347)	1328	(1318	1312)
$+\omega$(CH)	B_g	1357	(1351	1347)	1328	(1318	1313)
	A_u	1357	(1351	1346)	1327	(1319	1312)
	B_u	1356	(1351	1347)	1328	(1318	1312)

Modes[b]	Species	ν_{calc}/cm^{-1}						
$t(CH_2)$	A_g	1293	(1266	1262)				
	B_g	1293	(1266	1262)				
	A_u	1292	(1265	1261)				
	B_u	1292	(1264	1262)				
ν_{sk}(CC)	A_g	(1157	1151)	1145				
	B_g	(1157	1151)	1145				
	A_u	(1158	1150)	1145				
	B_u	(1158	1151)	1146				
ν_{sk}(CC)	A_g	(1108	1101)	1075				
$+\nu$(CMe)	B_g	(1108	1101)	1074				
	A_u	(1108	1100)	1075				
	B_u	(1108	1101)	1075				
ν(CMe)	A_g	(1057	1051)	1026				
$+\gamma$(Me)	B_g	(1057	1051)	1027				
	A_u	(1056	1050)	1025				
	B_u	(1056	1050)	1025				
γ(Me)	A_g	943	(921	920)	(916	912)	864	
	B_g	942	(921	920)	(916	911)	865	
	A_u	941	(921	920)	(916	911)	865	
	B_u	943	(921	920)	(916	912)	864	
$\gamma(CH_2)$	A_g	793	(776	774)				
	B_g	793	(777	774)				
	A_u	793	(778	774)				
	B_u	793	(777	774)				
ω(CMe)	A_g	(500	499)	(470	463)	443	374	
$+\delta$(CMe)	B_g	(500	497)	(470	465)	443	373	
	A_u	(502	497)	(468	463)	443	373	
	B_u	(502	498)	(467	463)	443	375	
δ(CC)	A_g	(308	300)	275				
$+\omega$(CMe)	B_g	(311	300)	272				
$+\delta$(CMe)	A_u	(313	295)	274				
	B_u	(311	296)	277				
τ(Me)	A_g	258	242	220				
	B_g	258	244	221				
	A_u	248	241	221				
	B_u	245	241	220				
τ(CC)	A_g	173	169	163	114	106		
$+\tau$(Me)	B_g	172	168	162	113	106		
	A_u	171	167	161	106	100		
	B_u	172	168	163	109	100		
Lattice	A_g	T_y81	R_z75	T_x40	T_z31			
Modes	B_g	R_z74	T_x58	T_y51	T_z44			
	A_u	R_z68	T_z30	T_x24	(T_y°0)			
	B_u	R_z63	T_y52	(T_x°0)	(T_z°0)			

[a] Vibrational modes of *E*-characters are enclosed in parentheses. The difference in wavenumber between a pair of such *E*-mode-like bands corresponds to site group splitting due to the lowering of molecular chain symmetry in the crystal lattice. The difference in wavenumber between the different symmetry species (vertical direction in this table) corresponds to the correlation splitting or Davidov splitting due to the intermolecular interactions. Refer to the text.

[b] Approximate expressions of normal modes. ν_a (CH_3), CH_3 antisymmetric stretching; ν(CH), CH stretching; ν_s (CH_3), CH_3 symmetric stretching; ν_a (CH_2), CH_2 antisymmetric stretching; $\nu_s(CH_2)$, CH_2 symmetric stretching; δ (CH_3): CH_3 bending; δ (CH_2), CH_2 bending; δ (CH), CH bending; w (CH_2): CH_2 wagging, w (CH), CH wagging; t (CH_2), CH_2 twisting; ν_{sk} (CC), skeletal CC stretching; ν (CMe), C–CH_3 stretching; γ(Me), CH_3 rocking; γ (CH_2), CH_2 rocking; w (CMe), C–CH_3 wagging; δ (CMe), C–CH_3 bending; δ (CC), skeletal CC bending; τ (Me), methyl torsion; τ (CC), skeletal CC torsion. In regard to the lattice modes, refer to Figure 4.

These modes are also easily affected by the change in intermolecular interactions. For example, Figure 8 shows variation of the vibrational frequencies calculated for the different unit cell parameters and/or the torsional angles of methyl groups. Among the various vibrational modes only the methyl torsional modes are affected sensitively by the change in these parameters or the change in the intermolecular interactions. The change in orderness of crystal structure is also predicted to affect this vibrational mode. For example, Figure 9 shows a comparison of far-infrared spectra measured for the samples prepared under different conditions. The sample annealed at 120°C corresponds to the disordered state according to ref 23. The sample annealed at 160°C corresponds to the ordered state. At liquid nitrogen temperature, the 160°C-annealed sample shows sharp bands in the region of $\tau(CH_3)$ and skeletal CC torsional modes. Especially the $\tau(CH_3)$ bands change their profile drastically; the change is more remarkable in the 160°C-annealed sample than in the 120°C-annealed sample. Melt-quenched sample shows much broader spectral profile even at liquid nitrogen temperature. Therefore we may consider that the sharp but complicated pattern of τ(Me) bands is characteristic of the ordered crystalline phase at low temperature and that the band profile is simpler for the less ordered crystal, reflecting the statistically disordered orientation of methyl groups.

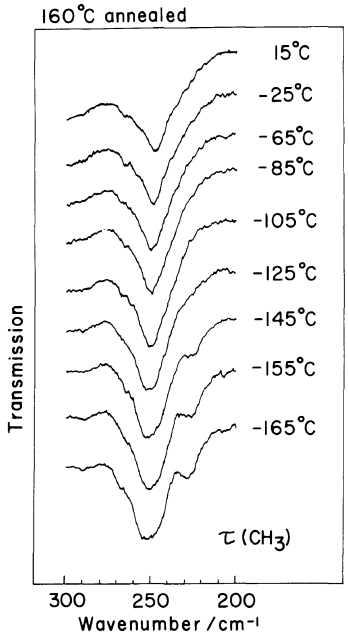

Figure 7. Temperature dependence of far-infrared spectra of unoriented it-PP film.

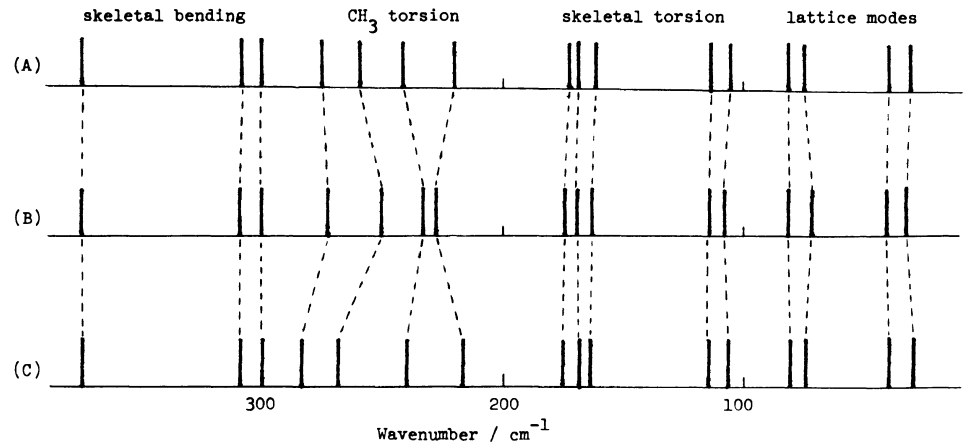

Figure 8. Variation of the vibrational frequencies depending on the unit cell parameters and torsional angles τ of methyl groups. (A) $a=6.65$ Å; $b=20.73$ Å; $c=6.50$ Å; $\beta=98.7°$; $\tau=71°$. (B) $a=6.65$ Å; $b=20.73$ Å; $c=6.50$ Å; $\beta=98.7°$; $\tau=60°$. (C) $a=6.67$ Å; $b=20.8$ Å; $c=6.50$ Å; $\beta=98.7°$; $\tau=75°$.

Corresponding to it, the bands of lattice modes are broader and weaker at room temperature and sharpened at liquid nitrogen temperature. The calculated vibrational frequencies of the external modes are in good agreement with the observed ones as seen in Figure 4.

B. Three-Dimensional Elastic Constants of it-PP Crystal

Three-dimensional elastic constant tensor c and compliance tensor s are calculated as shown below for the ordered structure.

$$c = \begin{bmatrix} 7.78 & 3.91 & 3.72 & 0.00 & 0.90 & 0.00 \\ 3.91 & 11.55 & 3.99 & 0.00 & -0.36 & 0.00 \\ 3.72 & 3.99 & 42.44 & 0.00 & -0.57 & 0.00 \\ 0.00 & 0.00 & 0.00 & 4.02 & 0.00 & -0.12 \\ 0.90 & -0.36 & -0.57 & 0.00 & 3.10 & 0.00 \\ 0.00 & 0.00 & 0.00 & -0.12 & 0.00 & 2.99 \end{bmatrix} \text{GPa} \quad (5)$$

$$s = \begin{bmatrix} 16.77 & -5.50 & -1.03 & 0.00 & -5.69 & 0.00 \\ -5.50 & 10.78 & -0.50 & 0.00 & 2.77 & 0.00 \\ -1.03 & -0.50 & 2.50 & 0.00 & 0.70 & 0.00 \\ 0.00 & 0.00 & 0.00 & 24.91 & 0.00 & 1.03 \\ -5.69 & 2.77 & 0.70 & 0.00 & 34.41 & 0.00 \\ 0.00 & 0.00 & 0.00 & 1.03 & 0.00 & 33.53 \end{bmatrix} \times 10^{-2}\,\text{GPa}^{-1} \quad (6)$$

Here the Cartesian coordinates are defined as follows: the x (1) axis $= a \sin \beta$, the y (2) axis $= b$ and the z (3) axis $= c$. Young's modulus along the chain axis and anisotropy of Young's modulus and linear compressibility in the plane perpendicular to the chain axis are discussed in the following on the basis of eq 5 and 6.

Young's Modulus and Linear Compressibility along the Chain Axis

Young's modulus E_c and linear compressibility β_c along the chain axis are given, respectively, by eq 7 and 8.

$$E_c = 1/s_{33} = 40.1 \text{ GPa} \quad (7)$$

$$\beta_c = s_{31} + s_{32} + s_{33} = 0.97 \times 10^{-2}\,\text{GPa}^{-1} \quad (8)$$

E_c is in excellent agreement with the values observed by the X-ray diffraction method (35 GPa[7] and 40—43 GPa[11]) and by the Raman LAM mode (37 GPa).[35] The calculated β_c is also in good agreement with the observed X-ray data, about $0.4 \times 10^{-2}\,\text{GPa}^{-1}$.[38,39]

Figure 10 shows the calculated distribution of strain energy among the intramolecular internal coordinates under application of tensile stress,[8] where the percentage for only one monomeric unit is shown for simplicity. In spite of the helical structure, a relatively large percentage of strain energy (*ca.* 55% in total) concentrates on the skeletal bond stretching and bond-angle deformation. Distribution of the energy to the skeletal torsional mode is about 30%. Such an energy distribution may come from the situation that the modulus was calculated for the polymer chain existing in the *crystal lattice* where the translational symmetry must be reserved even under deformation as long as an infinitesimally small external stress is considered. This constraint reduces the

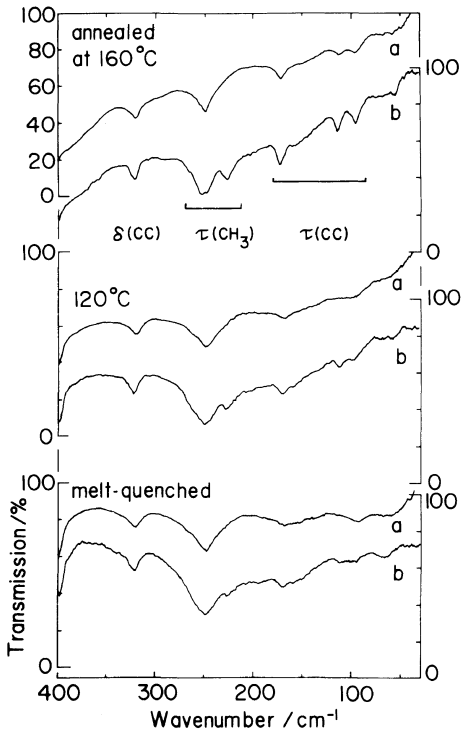

Figure 9. Far-infared spectra of unoriented it-PP compared among samples heat-treated under various conditions. Measurement temperatures are (a) room temperature and (b) liquid nitrogen temperature.

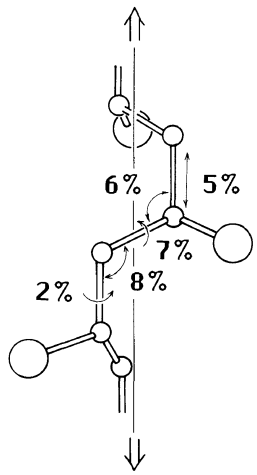

Figure 10. Calculated distribution of strain energy among various internal coordinates of it-PP chain under an application of tensile stress. For simplicity, the percentage for only one monomeric unit is shown here.

contribution of the torsional modes to some extent.[19,20,36] Another possibility is the characteristic conformation of it-PP chain. One of the skeletal CC bonds in the monomeric unit is almost parallel to the chain axis (CC_{axial}). This CC_{axial} bond and associated bond angle play an effective role in stretching the polymer chain, which reflects on the large energy distribution. The strain energy distribution among the intermolecular interactions is very small, an order of 0.01% at most. This may originate from the situation that most of the intermolecular interactions are between the methyl groups, which spread out of the skeletal chains just as likely as branches of trees, and so do not affect very much the deformation of skeletal main chain. In fact the E_c value calculated without any intermolecular interactions is 37.5 GPa, which is not much different from the E_c calculated with all the interactions included.

Anisotropy of Elastic Constants and Linear Compressibility in the Plane Perpendicular to the Chain Axis

Young's modulus $E(\theta)$ and linear compressibility $\beta(\theta)$ in the plane perpendicular to the chain axis are calculated by the following equations for the direction of angle θ from the x axis.

$$1/E(\theta) = s_{11}\cos^4\theta + s_{22}\sin^4\theta + (2s_{12}+s_{66})\sin^2\theta\cos^2\theta \quad (9)$$

$$\beta(\theta) = (s_{11}+s_{12}+s_{13})\cos^2\theta + (s_{21}+s_{22}+s_{23})\sin^2\theta \quad (10)$$

Figures 11(a) and 12(a) show, respectively, the calculated anisotropic curves of $E(\theta)$ and $\beta(\theta)$ in comparison with the data observed by the X-ray diffraction method.[37,38] The distance between the original point (center of the unit cell) and point on the curve represents the magnitude of E or β along this direction. As to the Young's modulus E, the calculated values are consistent in order with, but larger as a whole than, the observed values.[37] Of course, we need to consider the temperature

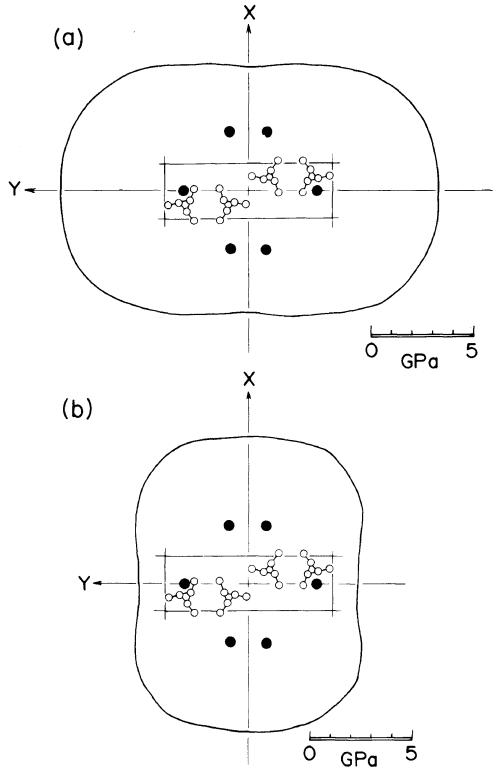

Figure 11. Anisotropic curve of Young's modulus in the plane perpendicular to the chain axis of it-PP crystal. (a) Calculated results using harmonic compliance constants in eq 6. (b) Calculated results using compliance constants modified by taking an anharmonic effect into account (refer to the text). The solid circles are X-ray observed values.[37]

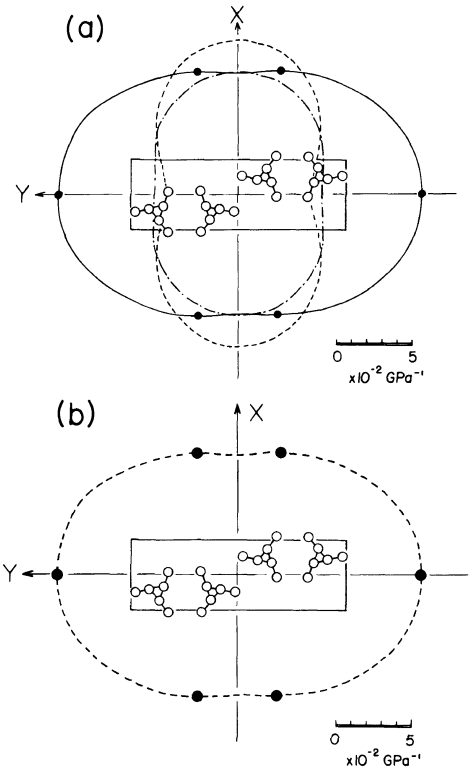

Figure 12. Anisotropic curve of linear compressibility in the plane perpendicular to the chain axis of it-PP crystal. (a) Solid curve and solid circles are observed data[38]: ------, calculated for the ordered crystal model ($P2_1/c$, eq 6); — - — - —, calculated for the disordered crystal model ($C2/c$, refer to the text). (b) Comparison between the observed data (●) and the curve (------) calculated by adjusting the mode Grüneisen constants γ_1 and γ_2 (refer to the text).

effect since the calculated values correspond to the moduli at low temperature while the observed values are at room temperature (the details will be discussed later). We must also consider the experimental problem of stress distribution in the bulk sample. In contrast to the case of the c axis (draw direction), the crystallite modulus in the lateral direction is not so different from the amorphous modulus and then an assumption of mechanical series model (equal stress working homogeneously on both the crystalline and amorphous phases) is difficult to apply. In other words, the crystallite modulus in the lateral direction may be dependent on the morphology of the sample more sensitively than the case along the chain axis. The X-ray method may thus contain some significant problems when quantitative comparison is made between the calculated and observed moduli in the lateral direction.

From such a point of view, the linear compressibility measured under hydrostatic pressure seems more reliable. But agreement in the anisotropy between the observed[38] and calculated compressibilities is not so good; the values along the x axis are almost equal whereas the values along the y axis are very different. In order to clarify the origin of this discrepancy, we calculated again the elastic constant tensors for the following several cases.

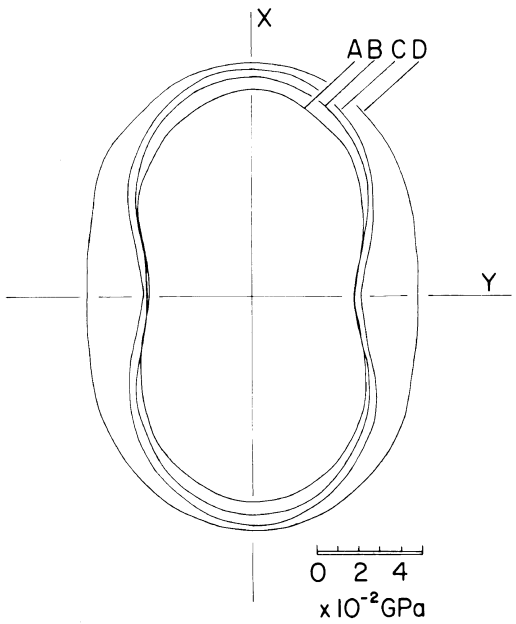

Figure 13. Variation of anisotropic curve of linear compressibility calculated for the various structural parameters, where only the harmonic terms are considered in the calculation of compliance tensors. A: $a=6.65$ Å; $b=20.73$ Å; $c=6.50$ Å; $\beta=98.7°$; $\tau=60°$. B: $a=6.65$ Å; $b=20.73$ Å; $c=6.50$ Å; $\beta=98.7°$; $\tau=71°$. C: $a=6.67$ Å; $b=20.8$ Å; $c=6.50$ Å; $\beta=98.7°$; $\tau=75°$. D: $a=6.65$ Å; $b=20.73$ Å; $c=6.50$ Å; $\beta=98.7°$; $\tau=71°$ but some of the intermolecular force constants are damped consciously (refer to the text).

(1) Unit cell parameters used in the calculation ($a=6.65$ Å and $b=20.73$ Å) are different from those of the samples actually used in the measurements: $a=6.66$ Å and $b=20.85$ Å (Ito[38]) or $a=6.67$ Å and $b=20.81$ Å (Nakafuku[39]). The latter are rather close to the parameters of the disordered phase ($a=6.67$ Å and $b=20.8$ Å).[23] The elastic constants were calculated for the disordered structure with an equal probability of upward and downward chains. The calculated anisotropic curve of linear compressibility is reproduced in Figure 12 (a). Anisotropy is not well modified by such a change. That is, the disorder in chain packing dose not affect very much the mechanical anisotropy in the lateral direction. Linear compressibility was calculated also for the ordered structure with various cell parameters as shown in Figure 13. But a slight change in the cell parameters gives only negligibly small effect on the anisotropy.

(2) Torsional angles of methyl groups were changed from $\tau=71°$ to 60° as a trial where the angle 60° is an energetically plausible value as frequently encounted in a gauche conformation. As seen in Figure 13, however, this modification is also negligible.

(3) In the calculation, some intermolecular H···H distances are appreciably short and give unreasonably large intermolecular force constant of *ca.* 0.03 mdyn Å^{-1}, an order of intramolecular torsional force constant. These large values were consciously modified to more reasonable values such as 0.01 mdyn Å^{-1}, for example. But even such a modification results in the anisotropic curve almost the same as the above calculated one, though compressibility itself increases to some extent.

(4) In the previous section, we pointed out the influence of thermally activated methyl rotation on the vibrational spectral feature. Such thermal fluctuation may make the force field of the crystal diffuse and decrease the intermolecular force constants. But as discussed above [(1)—(3)], change in the intermolecular interactions within an allowed range of modification did not lead to an essential revise of the elastic anisotropy as long as only the so-called harmonic effect was treated. The methyl groups rotating with large amplitude are speculated to lead to anharmonic behavior of the mechanical properties. This may be supported from the calculated result that application of hydrostatic pressure causes a strain energy distribution mainly on the H···H intermolecular interactions of the adjacent methyl groups (Figure 14). In general, elastic constants correspond to the initial slopes of acoustic phonon curves of the crystal. Lattice vibrational modes are considered to easily couple with acoustic phonons and so the anharmonic effects of lattice vibrational modes may be important in evaluating the abnormal

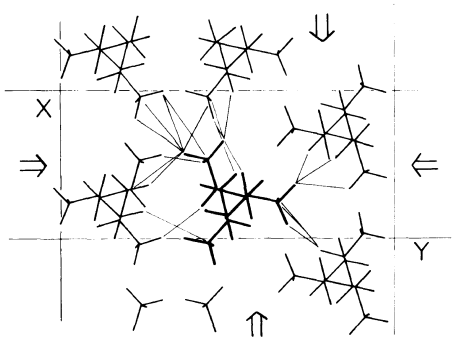

Figure 14. Calculated strain energy dsitrbution for it-PP crystal subjected to hydrostatic pressure. Thin solid lines connecting two hydrogen atoms of neighboring methyl groups indicate atomic pairs with relatively high percentage of strain energy (1—7%). In this figure, only pairs related to one asymmetric uint are given.

mechanical behavior of a crystal. But, as can be seen in the case of orthorhombic polyethylene crystal, the temperature effect of lattice vibrational modes is not so large in general and the anisotropic features of linear compressibility, *e.g.*, are not influenced by such an anharmonic effect of lattice vibrations except for some special cases: In other words, the mechanical anisotropy is almost determined by the structural features of the crystal. An extremely large discrepancy in the elastic anisotropy of linear compressibility (and Young's modulus) of it-PP crystal between the observed and calculated results may originate from another type of vibrational mode: the methyl torsional modes in the present case as discussed above. Therefore we may have an image such that the methyl torsinal modes couple with the acoustic modes and affect remarkably the slopes of acoustic dispersion curves through anharmonic effects. In the following, we estimate the contribution of such anharmonic effects of methyl modes coupled with acoustic phonons.

A Helmholtz free energy A of a crystal with a unit volume is expressed as a sum of static potential energy V and vibrational energy A_{vib};

$$A = V + A_{\mathrm{vib}} = V + (1/2)\sum_l h\nu_l + \sum_l \ln[1-\exp(-h\nu_l/kT)] \tag{11}$$

where ν_l is vibrational frequency of the lth mode, k is Boltzmann constant, h is Planck constant, and T is absolute temperature. The V and A_{vib} are assumed as functions of strain ε;

$$V = V_0 + (1/2)\sum_i\sum_j c_{ij}{}^0\varepsilon_i\varepsilon_j + (1/6)\sum_i\sum_j\sum_k c_{ijk}{}^0\varepsilon_i\varepsilon_j\varepsilon_k + \cdots \tag{12}$$

$$\begin{aligned} A_{\mathrm{vib}} &= A_0 + \sum_i (\partial A_{\mathrm{vib}}/\partial\varepsilon_i)_0\varepsilon_i \\ &\quad + (1/2)\sum_i\sum_j (\partial^2 A_{\mathrm{vib}}/\partial\varepsilon_i\partial\varepsilon_j)_0\varepsilon_i\varepsilon_j + \cdots \\ &= A_0 - \sum_i\sum_l E_l\gamma_{il}\varepsilon_i \\ &\quad + (1/2)\sum_i\sum_j\sum_l [\gamma_{il}\gamma_{jl}(E_l - TC_{vl}) \\ &\quad - E_l(\partial\gamma_{il}/\partial\varepsilon_j)]\varepsilon_i\varepsilon_j + \cdots \end{aligned} \tag{13}$$

Here

$$E_l = (1/2)h\nu_l + h\nu_l/[\exp(h\nu_l/kT)-1] \tag{14}$$

$$C_{vl} = k(h\nu_l/kT)^2\exp(h\nu_l/kT)/[\exp(h\nu_l/kT)-1]^2 \tag{15}$$

$$\gamma_{il} = -(\partial\nu_l/\partial\varepsilon_i)_0/\nu_l \tag{16}$$

E_l is a vibrational internal energy, C_{vl} is a vibrational heat capacity, and γ_{il} is a mode Grüneisen constant for the lth mode under the strain ε_i. An isothermal elastic constant $c_{ij}{}^{\mathrm{T}}$ may be given as follows in a quasiharmonic approximation.

$$\begin{aligned} c_{ij}{}^{\mathrm{T}} &= (\partial^2 A/\partial\varepsilon_i\partial\varepsilon_j)^{\mathrm{T}} \\ &\approx c_{ij}{}^0 + \sum_l [\gamma_{il}\gamma_{jl}(E_l - C_{vl}T) - E_l(\partial\gamma_{il}/\partial\varepsilon_j)] \end{aligned} \tag{17}$$

In general the vibrational frequency ν_l changes almost linearly with increase of external strain ε_i:[20]

$$\nu_l \approx \nu_l{}^0 - (\partial \nu_l/\partial \varepsilon_i)_0 \varepsilon_i \,. \tag{18}$$

Therefore $(\partial \gamma_{il}/\partial \varepsilon_j)$ in eq 17 may be approximated as

$$(\partial \gamma_{il}/\partial \varepsilon_j) \approx \gamma_{il}\gamma_{jl} \tag{19}$$

In a high temperature approximation, $E_l \approx kT$ and $C_{vl} \approx k$, and then eq 17 becomes as below.

$$c_{ij}{}^{\mathrm{T}} \approx c_{ij}{}^{\circ} - kT\sum_l \gamma_{il}\gamma_{jl} \approx c_{ij}{}^{\circ} - kTN\gamma_i\gamma_j \tag{20}$$

As stated above, the methyl torsional modes coupled with acoustic (or elastic) phonons are considered to contribute greatly to the temperature dependence of elastic constants. Therefore we assume here that only these modes are involved in eq 20. The last equation in eq 20 represents this approximation and subscript l is omitted where N is the number of methyl torsional modes involved in the unit volume of crystal. The compliance tensor $\boldsymbol{s}^{\mathrm{T}}$ is obtained as an inverse of elastic constant tensor $\boldsymbol{c}^{\mathrm{T}}$. As shown below, elastic contant tensors can be classified into two symmetry species A_{g} and B_{g} in the present case.

$$\boldsymbol{c}^{A_{\mathrm{g}}} = \begin{bmatrix} c_{11} & c_{12} & c_{13} & 0 & c_{15} & 0 \\ c_{21} & c_{22} & c_{23} & 0 & c_{25} & 0 \\ c_{31} & c_{32} & c_{33} & 0 & c_{35} & 0 \\ 0 & 0 & 0 & 0 & 0 & 0 \\ c_{51} & c_{52} & c_{53} & 0 & c_{55} & 0 \\ 0 & 0 & 0 & 0 & 0 & 0 \end{bmatrix}$$

$$\boldsymbol{c}^{B_{\mathrm{g}}} = \begin{bmatrix} 0 & 0 & 0 & 0 & 0 & 0 \\ 0 & 0 & 0 & 0 & 0 & 0 \\ 0 & 0 & 0 & 0 & 0 & 0 \\ 0 & 0 & 0 & c_{44} & 0 & c_{46} \\ 0 & 0 & 0 & 0 & 0 & 0 \\ 0 & 0 & 0 & c_{64} & 0 & c_{66} \end{bmatrix} \tag{21}$$

In the calculation of $E(\theta)$ and $\beta(\theta)$ in eq 9 and 10, we may focus on the $\boldsymbol{c}^{A_{\mathrm{g}}}$ matrix alone. An analytical derivation of $\boldsymbol{s}^{A_{\mathrm{g}}}$ as $(\boldsymbol{c}^{A_{\mathrm{g}}})^{-1}$ is difficult to carry out. In order to conduct the calculation as simply as possible without any loss of essential feature, we neglect here the components c_{i5} in the $\boldsymbol{c}^{A_{\mathrm{g}}}$ matrix and calculate the inverse matrix of the $(c_{ij})^{A_{\mathrm{g}}}$ matrix with i and $j=1$ to 3. Final expressions for $s_{ij}{}^{\mathrm{T}}$ may be given as follows assuming that the higher terms of γ^4 etc. may be neglected because of their small magnitude.

$$s_{ij}{}^{\mathrm{T}} \approx s_{ij}{}^{\circ} + kTNp_{ij}/q^2 \tag{20}$$

where i and j range from 1 to 3. The coefficients p_{ij} and q are expressed as below using the harmonic elastic components $c_{ij}{}^{\circ}$.

$$\begin{aligned}
p_{11} &= w(c_{22}{}^{\circ}c_{33}{}^{\circ} - c_{23}{}^{\circ}c_{23}{}^{\circ}) \\
&\quad - q(c_{33}{}^{\circ}\gamma_2{}^2 + c_{22}{}^{\circ}\gamma_3{}^2 - 2c_{23}{}^{\circ}\gamma_2\gamma_3) \\
p_{22} &= w(c_{11}{}^{\circ}c_{33}{}^{\circ} - c_{13}{}^{\circ}c_{13}{}^{\circ}) \\
&\quad - q(c_{33}{}^{\circ}\gamma_1{}^2 + c_{11}{}^{\circ}\gamma_3{}^2 - 2c_{13}{}^{\circ}\gamma_1\gamma_3) \\
p_{33} &= w(c_{11}{}^{\circ}c_{22}{}^{\circ} - c_{12}{}^{\circ}c_{12}{}^{\circ}) \\
&\quad - q(c_{22}{}^{\circ}\gamma_1{}^2 + c_{11}{}^{\circ}\gamma_2{}^2 - 2c_{12}{}^{\circ}\gamma_1\gamma_2) \\
p_{23} &= w(c_{12}{}^{\circ}c_{13}{}^{\circ} - c_{11}{}^{\circ}c_{23}{}^{\circ}) \\
&\quad - q(c_{12}{}^{\circ}\gamma_1\gamma_3 + c_{13}{}^{\circ}\gamma_1\gamma_2 \\
&\quad - c_{11}{}^{\circ}\gamma_2\gamma_3 - c_{23}{}^{\circ}\gamma_1{}^2) \\
p_{13} &= w(c_{12}{}^{\circ}c_{33}{}^{\circ} - c_{13}{}^{\circ}c_{22}{}^{\circ}) \\
&\quad - q(c_{23}{}^{\circ}\gamma_1\gamma_2 + c_{12}{}^{\circ}\gamma_2\gamma_3 \\
&\quad - c_{22}{}^{\circ}\gamma_1\gamma_3 - c_{13}{}^{\circ}\gamma_2{}^2) \\
p_{12} &= w(c_{13}{}^{\circ}c_{23}{}^{\circ} - c_{12}{}^{\circ}c_{33}{}^{\circ}) \\
&\quad - q(c_{13}{}^{\circ}\gamma_2\gamma_3 + c_{23}{}^{\circ}\gamma_1\gamma_3 \\
&\quad - c_{33}{}^{\circ}\gamma_1\gamma_2 - c_{12}{}^{\circ}\gamma_3{}^2) \\
q &= c_{11}{}^{\circ}c_{22}{}^{\circ}c_{33}{}^{\circ} + 2c_{12}{}^{\circ}c_{23}{}^{\circ}c_{13}{}^{\circ} \\
&\quad - c_{22}{}^{\circ}c_{13}{}^{\circ}c_{13}{}^{\circ} - c_{11}{}^{\circ}c_{23}{}^{\circ}c_{23}{}^{\circ} \\
&\quad - c_{13}{}^{\circ}c_{12}{}^{\circ}c_{12}{}^{\circ} \\
w &= (c_{23}{}^{\circ}c_{33}{}^{\circ} - c_{23}{}^{\circ 2})\gamma_1{}^2 + (c_{11}{}^{\circ}c_{33}{}^{\circ} \\
&\quad - c_{13}{}^{\circ 2})\gamma_2{}^2 + (c_{11}{}^{\circ}c_{22}{}^{\circ} - c_{12}{}^{\circ 2})\gamma_3{}^2 \\
&\quad + 2(c_{13}{}^{\circ}c_{23}{}^{\circ} - 2c_{33}{}^{\circ}c_{12}{}^{\circ})\gamma_1\gamma_2 + (2c_{12}{}^{\circ}c_{13}{}^{\circ}
\end{aligned}$$

$$-2c_{11}{}^{\circ}c_{23}{}^{\circ})\gamma_2\gamma_3+(2c_{12}{}^{\circ}c_{23}{}^{\circ} -2c_{22}{}^{\circ}c_{13}{}^{\circ})\gamma_1\gamma_3 \quad (21)$$

Thus the linear compressibilty at a temparature T may be expressed as follows.

$$\begin{aligned}\beta_1{}^{\mathrm{T}} &= s_{11}{}^{\mathrm{T}}+s_{12}{}^{\mathrm{T}}+s_{13}{}^{\mathrm{T}} \\ &\approx \beta_1{}^{\circ}+(kTN/q^2)(u_{11}\gamma_1{}^2+u_{12}\gamma_2{}^2+u_{13}\gamma_3{}^2 \\ &\quad +u_{14}\gamma_2\gamma_3+u_{15}\gamma_1\gamma_3+u_{16}\gamma_1\gamma_2) \\ \beta_2{}^{\mathrm{T}} &= s_{21}{}^{\mathrm{T}}+s_{22}{}^{\mathrm{T}}+s_{23}{}^{\mathrm{T}} \\ &\approx \beta_2{}^{\circ}+(kTN/q^2)(u_{21}\gamma_1{}^2+u_{22}\gamma_2{}^2+u_{23}\gamma_3{}^2 \\ &\quad +u_{24}\gamma_2\gamma_3+u_{25}\gamma_1\gamma_3+u_{26}\gamma_1\gamma_2) \end{aligned} \quad (22)$$

where

$$\begin{aligned}\beta_1{}^{o} &= s_{11}{}^{\circ}+s_{12}{}^{\circ}+s_{13}{}^{\circ} \\ \beta_2{}^{\circ} &= s_{21}{}^{\circ}+s_{22}{}^{\circ}+s_{23}{}^{\circ} \\ u_{11} &= g_1(c_{22}{}^{\circ}c_{33}{}^{\circ}-c_{23}{}^{\circ 2}) \\ u_{12} &= g_1(c_{11}{}^{\circ}c_{33}{}^{\circ}-c_{13}{}^{\circ 2})-q(c_{33}{}^{\circ}-c_{13}{}^{\circ}) \\ u_{13} &= g_1(c_{11}{}^{\circ}c_{22}{}^{\circ}-c_{12}{}^{\circ 2})-q(c_{22}{}^{\circ}-c_{12}{}^{\circ}) \\ u_{14} &= g_1(2c_{12}{}^{\circ}c_{13}{}^{\circ}-2c_{11}{}^{\circ}c_{23}{}^{\circ}) \\ &\quad -q(c_{13}{}^{\circ}+c_{12}{}^{\circ}-2c_{23}{}^{\circ}) \\ u_{15} &= g_1(2c_{12}{}^{\circ}c_{23}{}^{\circ}-2c_{22}{}^{\circ}c_{13}{}^{o}) \\ &\quad -q(c_{23}{}^{\circ}-c_{22}{}^{\circ}) \\ u_{16} &= g_1(2c_{13}{}^{\circ}c_{23}{}^{\circ}-2c_{33}{}^{\circ}c_{12}{}^{o}) \\ &\quad -q(c_{23}{}^{\circ}-c_{33}{}^{\circ}) \\ u_{21} &= g_2(c_{22}{}^{\circ}c_{33}{}^{\circ}-c_{23}{}^{\circ 2})-q(c_{33}{}^{\circ}-c_{23}{}^{\circ}) \\ u_{22} &= g_2(c_{11}{}^{\circ}c_{33}{}^{\circ}-c_{13}{}^{\circ 2}) \\ u_{23} &= g_2(c_{11}{}^{\circ}c_{22}{}^{\circ}-c_{12}{}^{\circ 2})-q(c_{11}{}^{\circ}-c_{12}{}^{\circ}) \\ u_{24} &= g_2(2c_{12}{}^{\circ}c_{13}{}^{\circ}-2c_{11}{}^{\circ}c_{23}{}^{\circ}) \\ &\quad -q(c_{13}{}^{\circ}-c_{11}{}^{\circ}) \\ u_{25} &= g_2(2c_{12}{}^{\circ}c_{23}{}^{\circ}-2c_{22}{}^{\circ}c_{13}{}^{\circ}) \\ &\quad -q(c_{23}{}^{\circ}+c_{12}{}^{o}-2c_{13}{}^{\circ}) \\ u_{26} &= g_2(2c_{13}{}^{\circ}c_{23}{}^{\circ}-2c_{33}{}^{\circ}c_{12}{}^{\circ}) \\ &\quad -q(c_{13}{}^{\circ}-c_{33}{}^{\circ}) \\ g_1 &= c_{22}{}^{\circ}c_{33}{}^{\circ}+c_{13}{}^{\circ}c_{23}{}^{\circ}+c_{12}{}^{\circ}c_{23}{}^{\circ}-c_{23}{}^{\circ 2} \\ &\quad -c_{12}{}^{\circ}c_{33}{}^{\circ}-c_{13}{}^{\circ}c_{22}{}^{\circ} \\ g_2 &= c_{13}{}^{\circ}c_{23}{}^{\circ}+c_{11}{}^{\circ}c_{33}{}^{\circ}+c_{12}{}^{\circ}c_{13}{}^{\circ}-c_{12}{}^{\circ}c_{33}{}^{\circ} \\ &\quad -c_{13}{}^{\circ 2}-c_{11}{}^{\circ}c_{23}{}^{\circ} \end{aligned} \quad (23)$$

By the numerical values of $c_{ij}{}^{\circ}$ and $s_{ij}{}^{\circ}$ in eq 5, $T=300\,\mathrm{K}$ and $N=12/v_c$ (12 is a number of methyl torsional modes involved in the unit cell with a volume v_c), we may get the following equations under assumption of $\gamma_3=0$. (This assumption is not unreasonable because the shift in vibrational frequency caused by a tensile strain along the chain axis is considered very small for the torsional modes of methyl side groups).

$$\begin{aligned}\beta_1{}^{\mathrm{T}} &= 10.24+0.061\gamma_1{}^2-0.020\gamma_2{}^2 \\ &\quad +0.021\gamma_1\gamma_2\ (\times 10^{-2}\ \mathrm{GPa}^{-1}) \\ \beta_2{}^{\mathrm{T}} &= 4.78-0.029\gamma_1{}^2+0.020\gamma_2{}^2 \\ &\quad +0.041\gamma_1\gamma_2\ (\times 10^{-2}\ \mathrm{GPa}^{-1}) \end{aligned} \quad (24)$$

By adjusting the Grüneisen constants γ_1 and γ_2, we may fit the observed anisotropic curve of linear compressibility shown in Figure 12(b) on the basis of eq 10. The obtained γ_1 and γ_2 are

$$\begin{aligned}\gamma_1 &= 4.65 \\ \gamma_2 &= 15.91 \end{aligned} \quad (25)$$

In other words, a larger value of γ_2 than γ_1 is required to reproduce the mechanical anisotropy of it-PP crystal at room temperature. Using these Grüneisen constants, we can estimate $s_{11}{}^{\mathrm{T}}$, $s_{12}{}^{\mathrm{T}}$, and $s_{22}{}^{\mathrm{T}}$ in eq 9 as $s_{11}{}^{\mathrm{T}}=14.02\times10^{-2}\,\mathrm{GPa}^{-1}$, $s_{12}{}^{\mathrm{T}}=-5.07\times10^{-2}\,\mathrm{GPa}^{-1}$, and $s_{22}{}^{\mathrm{T}}=18.70\times10^{-2}\,\mathrm{GPa}^{-1}$. The anisotropic curve of Young's modulus $E(\theta)$ can be calculated by eq 9 where $s_{66}{}^{\mathrm{T}}$ is assumed to be equal to $s_{66}{}^{\circ}$. The result is shown in Figure 11(b). The calculated curve is closer to the observed one when compared with the originally calculated curve.

The Grüneisen constants γ_1 and γ_2 calculated for methyl torsional mode are not unreasonable judging from the large frequency shift induced by a slight change in the unit cell parameters a and b as shown in Figure 8. From this figure, the Grüneisen constant is roughly estimated as 6—11, this being close to the above determined values.

By these Grüneisen constants, we may also evaluate the linear thermal expansion coeffi-

cients α_1 and α_2 along the x and y axes, respectively. From eqs 11 and 12, α_i may be expressed approximately as follows.

$$\alpha_i = \sum_j s_{ij}{}^{\mathrm{T}} \left(\sum_l C_{vl} \gamma_{jl} \right) = kN \sum_j s_{ij}{}^{\mathrm{T}} \gamma_j \qquad (26)$$

Using the above $s_{ij}{}^{\mathrm{T}}$ and γ_j, we have

$$\alpha_1 = -0.29 \times 10^{-4}\,\mathrm{K}^{-1}$$
$$\alpha_2 = 5.12 \times 10^{-4}\,\mathrm{K}^{-1} \qquad (27)$$

The reported experimental data are $\alpha_1 = 0.5 - 1.0 \times 10^{-4}\,\mathrm{K}^{-1}$ and $\alpha_2 = 1.6 - 2.3 \times 10^{-4}\,\mathrm{K}^{-1}$.[39,40] The calculated values of α_1 and α_2 and their relative amplitudes are of the same order as those observed but the ageeement is not so good. This difference in α_i between the observed and calculated values might come from a neglection of other types of lattice vibrational modes in eq 26.

CONCLUSION

In this paper, we calculated the vibrational frequencies and three-dimensional elastic constants of it-PP crystal using the lattice dynamical technique. The calculated vibrational frequencies agree well with the spectra observed at low temperature. The far-infrared bands of methyl torsional modes change their spectral pattern drastically as the temperature varies below and above *ca.* -145°C where the methyl rotational motion begins to occur. The methyl torsional mode is considered to couple with acoustic phonons through the anharmonic effect and affect the anisotropy in the mechanical property of it-PP crystal, particularly of the anisotropy in the lateral direction. By taking such an effect into account, we have derived an approximate estimation of isothermal elastic constants and compliance tensors on the basis of an idea of mode Grüneisen constant. As can be seen from a discrepancy in the thermal expansibility between the observed and calculated values, we should consider the anharmonic contribution of all internal and external vibrational modes when estimating mechanical anisotropy. But, as long as we are concerned with the mechanical anisotropy in the lateral direction, the methyl torsional modes coupled with acoustic phonons are reasonably considered to make an essentially important contribution. One of the most direct experimental methods to check the above discussion may be measurement of anisotropic elastic constants at low temperature where the large amplitude of methyl rotation is suppressed and so the harmonically-predicted original anisotropy in $E(\theta)$ and $\beta(\theta)$ [Figures 11 and 12] should be observed.

Acknowledgements. The authors thank Mitsui Petrochemical Industries, Co., Ltd. and Sumitomo Chemical Industries, Co., Ltd. in Japan for their supply of it-PP samples.

REFERENCES

1. A. Ciferri and I. M. Ward, Ed., "Ultra-High Modulus Polymer," Applied Science Publishers, London, 1979.
2. I. M. Ward, Ed. "Developments in Oriented Polymer," Elsevier Applied Science, London, 1987.
3. "The Materials Science and Engineering of Rigid-Rod Polymers," Symposium Proceedings of Material Research Society, Vol. 134, Material Research Society, 1989.
4. P. G. Lenhart and W. W. Adams, Symposium Proceedings of Material Research Society, Vol. 134, Material Research Society, 1989, p 329.
5. K. Tashiro and M. Kobayashi, *Macromolecules*, **24**, 3706 (1991).
6. M. Matsuo and C. Sawatari, *Macromolecules*, **19**, 2036 (1986).
7. I. Sakurada, K. Kaji, *J. Polym. Sci., C*, **31**, 57 (1970).
8. K. Tashiro, M. Kobayashi, and H. Tadokoro, *Macromolecules*, **11**, 914 (1978).
9. A. Peguy and R. St. John Manley, *Polym. Commun.*, **25**, 39 (1984).
10. M. Matsuo and C. Sawatari, *Polym. J.*, **18**, 759 (1986).
11. C. Sawatari and M. Matsuo, *Macromolecules*, **19**, 2653 (1986).
12. R. F. Shcaufele and T. Shimanouchi, *J. Am. Chem. Soc.*, **47**, 3605 (1967).
13. L. Holliday and J. W. White, *Pure Appl. Chem.*, **26**, 545 (1971).
14. K. Tashiro and H. Tadokoro, "Encyclopedia of Polymer Science and Engineering," Supplement,

John Wiley & Sons, Inc., New York, 1989, p 187.
15. K. Tashiro, M. Kobayashi, and H. Tadokoro, *Macromolecules*, **11**, 908 (1978).
16. K. Tashiro and H. Tadokoro, *Macromolecules*, **14**, 781 (1981).
17. K. Tashiro, M. Kobayashi, and H. Tadokoro, *Ferroelectrics*, **32**, 167 (1981).
18. K. Tashiro and M. Kobayashi, *Polymer*, **32**, 1516 (1991).
19. K. Tashiro, M. Kobayashi, and H. Tadokoro, *Macromolecules*, **10**, 413 (1977).
20. K. Tashiro, G. Wu, and M. Kobayashi, *J. Polym. Sci., B, Polym. Phys.*, **28**, 2527 (1990).
21. G. Natta and P. Corradini, *Suppl. Nuovo Cimento*, **15**, 40 (1960).
22. Z. Mencik, *J. Macromol. Sci., Phys.*, **136**, 101 (1972).
23. M. Hikosaka and T. Seto, *Polym. J.*, **5**, 11 (1973).
24. R. G. Snyder and J. H. Schachtshneider, *Spectrochim. Acta*, **20**, 853 (1964).
25. T. Miyazawa, *J. Polym. Sci., C*, **7**, 59 (1964).
26. H. Tadokoro, M. Kobayashi, M. Ukita, K. Yasufuku, S. Murahashi, and T. Torii, *J. Chem. Phys.*, **42**, 1432 (1965).
27. G. Zerbi and L. Piseri, *J. Chem. Phys.*, **49**, 3840 (1968).
28. G. V. Fraser, P. J. Hendra, D. S. Watson, M. J. Gall, H. A. Willis, and M. E. A. Gudby, *Spectrochim. Acta*, **29A**, 1525 (1973).
29. M. Goldstein, M. E. Seeley, H. A. Willis, and V. J. I. Zichy, *Polymer*, **14**, 530 (1973).
30. H. Tadokoro, "Structure of Crystalline Polymers," John-Wiley, New York, N. Y., 1979.
31. D. E. Williams, *J. Chem. Phys.*, **45**, 3770 (1966).
32. D. E. Williams, *J. Chem. Phys.*, **47**, 4680 (1967).
33. Y. Ishida and K. Yamafuji, *Koll. Z. Z. Polym.*, **177**, 97 (1961).
34. D. R. Beckett, J. M. Chalmers, M. W. Mackenzie, H. A. Willis, H. G. Edwards, J. S. Lees, and D. A. Long, *Eur. Polym. J.*, **21**, 849 (1985).
35. S. L. Hsu, S. Krimm, S. Krause, and G. S. Y. Yeh, *J. Polym. Sci. Polym. Lett. Ed.*, **14**, 195 (1976).
36. K. Tashiro, S. Minami, G. Wu, and M. Kobayashi, *J. Polym. Sci, B, Polym. Phys.*, in press.
37. I. Sakurada and K. Kaji, *Makromol. Chem. Suppl.* **1**, 599 (1975).
38. T. Ito, *Polymer*, **23**, 1412 (1982).
39. C. Nakafuku, *Polym. Prepr. Jpn.*, **28**, 440 (1979).
40. K. Nakamae, T. Nishino, K. Hata, and T. Matsumoto, *Koubunshi Ronbunshu*, **42**, 241 (1985).